Published in final edited form as:

Stem Cell Res. 2016 May ; 16(3): 740–750. doi:10.1016/j.scr.2016.04.014.

Cell alignment induced by anisotropic electrospun fibrous scaffolds alone has limited effect on cardiomyocyte maturation

Jingjia Han[a,b], **Qingling Wu**[a,c], **Younan Xia**[b,c,d], **Mary B Wagner**[a,c], and **Chunhui Xu**[a,b,c,*]

[a]Division of Pediatric Cardiology, Department of Pediatrics, Emory University School of Medicine and Children's Healthcare of Atlanta, Atlanta, GA 30322, USA

[b]Parker H. Petit Institute for Biotechnology and Bioscience, Georgia Institute of Technology, Atlanta, GA 30332, USA

[c]The Wallace H. Coulter Department of Biomedical Engineering, Georgia Institute of Technology and Emory University, Atlanta, GA 30332, USA

[d]School of Chemistry and Biochemistry, Georgia Institute of Technology, Atlanta, GA 30332, USA

Abstract

Enhancing the maturation of human pluripotent stem cell-derived cardiomyocytes (hPSC-CMs) will facilitate their applications in disease modeling and drug discovery. Previous studies suggest that cell alignment could enhance hPSC-CM maturation; however, the robustness of this approach has not been well investigated. To this end, we examined if the anisotropic orientation of hPSC-CMs imposed by the underlying aligned fibers within a 3D microenvironment could improve the maturation of hPSC-CMs. Enriched hPSC-CMs were cultured for two weeks on Matrigel-coated anisotropic (aligned) and isotropic (random) polycaprolactone (PCL) fibrous scaffolds, as well as tissue culture polystyrenes (TCPs) as a control. As expected, hPSC-CMs grown on the two types of fibrous scaffolds exhibited anisotropic and isotropic orientations, respectively. Similar to cells on TCPs, hPSC-CMs cultured on these scaffolds expressed CM-associated proteins and were pharmacologically responsive to adrenergic receptor agonists, a muscarinic agonist, and a gap junction uncoupler in a dose-dependent manner. Although hPSC-CMs grown on anisotropic fibrous scaffolds displayed the highest expression of genes encoding a number of sarcomere proteins, calcium handling proteins and ion channels, their calcium transient kinetics were slower than cells grown on TCPs. These results suggest that electrospun anisotropic fibrous scaffolds, as a single method, have limited effect on improving the maturation of hPSC-CMs.

*Corresponding author at: Department of Pediatrics, Emory University School of Medicine, 2015 Uppergate Drive, Atlanta, GA 30322, USA. chunhui.xu@emory.edu (C. Xu).

Supplementary data to this article can be found online at http://dx.doi.org/10.1016/j.scr.2016.04.014.

Author contributions

J.H. conceived and designed the study, performed experiments, analyzed and interpreted the data, and wrote the manuscript. Q.W. performed experiments and analyzed the data, and reviewed the manuscript. Y.X. provided guidance, experimental reagents, and instruments for the preparation of electrospun fibers, and revised the manuscript. M.B.W. provided guidance, experimental reagents, equipment, and analytical tools for the MEA recording and calcium imaging, and revised the manuscript. C.X. conceived and oversaw the study, and revised the manuscript.

Conflict of interests

The authors declare that there is no conflict of interests.

Keywords

Cardiomyocyte; Electrospinning; Maturation; Scaffold; Stem cell

1. Introduction

Human pluripotent stem cell (hPSC)-derived cardiomyocytes (CMs) have provided a realistic and exciting platform for drug-induced toxicity screening and disease modeling (Burridge et al., 2012; Yang et al., 2014). Directed differentiation of CMs from hPSCs has been established in several laboratories (reviewed in (Burridge et al., 2012; Mummery et al., 2012)), producing immature CMs that have limited ability to accurately reflect the physiology and pathology of human hearts (Nunes et al., 2013; Yang et al., 2014). Evidence suggests hPSC-CMs can progressively mature in long-term culture (Kamakura et al., 2013; Lundy et al., 2013), but this method can be time consuming which may limit its utility. Thus, new approaches that enhance hPSC-CM maturation are needed.

In adult myocardium, CMs are longitudinally aligned in the form of parallel bundles to facilitate the mechanical contraction and electrical propagation of the heart tissue. Mimicking nature's work, engineered anisotropy (namely cell patterning) has been widely used as an effective approach to improve the maturation of immature CMs (Yang et al., 2014). This engineered anisotropy can be induced by electrical (Nunes et al., 2013; Radisic et al., 2004) or mechanical loading (Thavandiran et al., 2013; Tulloch et al., 2011) and also by substrates that provide topographical guidance, which create a permissive environment to guide the alignment of CMs (Chen et al., 2014; Kim et al., 2010; Liau et al., 2011; Ma et al., 2014; McCain et al., 2014; Rao et al., 2013; Salick et al., 2014; Zhang et al., 2013). Aligned CMs may result in enhanced cardiac phenotypes indicative of cell maturation. Recently, enhanced sarcomere alignment (Khan et al., 2015; Salick et al., 2014), excitation-contraction coupling (Zhang et al., 2013), calcium cycling (Khan et al., 2015; Rao et al., 2013), and drug sensitivity (Chen et al., 2014) have been reported for hPSC-CMs grown on various micro-patterned substrates, suggesting improved cell structural and/or functional maturation. However, the robustness of cell alignment as a single approach to improve the maturation of hPSC-CMs has not been fully investigated.

Electrospinning is an effective platform technique to produce anisotropic (aligned) fibrous scaffolds (Barnes et al., 2007), comparing to conventional methods in fabricating aligned substrates, such as soft lithography (Kim et al., 2010; McCain et al., 2014; Rao et al., 2013; Salick et al., 2014), photolithography, two-photon initiated polymerization (Ma et al., 2014), and micro-fluidics (Xiao et al., 2014). Importantly, the as-prepared electrospun scaffolds possess a fibrous structure resembling the native extracellular matrix (ECM), a high surface-to-volume ratio, and a tunable porosity (Li et al., 2002). Remarkably, those fibrous meshes can be easily fabricated with distinct anisotropy through the use of a non-conductive template, as the surface topography and architecture of the non-conductive template is readily transferrable (Senel Ayaz et al., 2014; Zhao et al., 2013). A recent study has shown that using a textile-templated electrospun aligned PU scaffold as the substrate, neonatal rat CMs displayed more stable and prolonged spontaneous syncytium, comparing with cells on

tissue culture polystyrenes (TCPs) (Senel Ayaz et al., 2014). Based on these findings, we examined whether aligned electrospun fibrous scaffolds could induce the anisotropic cell alignment and improve the maturation of hPSC-CMs.

To this end, we first prepared the aligned and isotropic (random) polycaprolactone (PCL) fibrous scaffolds, and confirmed the anisotropic and isotropic alignment of hPSC-CMs cultured on these substrates coated with Matrigel, including the use of TCPs as a control. We then evaluated the structural, molecular and functional properties of the cells after 2 weeks culture on each type of substrates. Our results show that aligned electrospun fibrous scaffolds can induce the anisotropic cell alignment of hPSC-CMs but do not improve the maturation of hPSC-CMs.

2. Materials and methods

2.1. Preparation and characterization of electrospun fibrous scaffolds

Electrospun fibrous scaffolds were prepared as previously described (Cipitria et al., 2011; Xie et al., 2009). In brief, 11% (*w*/*v*) PCL solution was prepared by dissolving PCL (MW 75,000–90,000, cat No. 440744, Sigma-Aldrich) in 1,1,1,3,3,3-Hexafluoro-2-propanol (HFP, cat No. 105228, Sigma-Aldrich). After mixing for at least 10 h, the solution was loaded into a 5-mL BD plastic syringe equipped with a blunt 22-gauge needle. The solution-loaded syringe was mounted into a syringe pump (KDS-200, Stoelting) where the flow rate was set at 3.0 mL/h and 1.8 mL/h to produce aligned and random fibers, respectively. The needle was connected to the positive output of a high-voltage power supply (ES30P-5W, Gamma High Voltage Research, Inc.) set at 13 kV. The collector, a custom-made rotating mandrel, was grounded and set to rotate at different speeds by adjusting the potential to 7 V and 1 V to fabricate aligned and random fibers, respectively. The distance between the needle tip and the collector was set at 25 cm. After approximately 1–1.5 h of collection, the fibrous mat (~100 μm in thickness) was released from the collector and stored under a chemical hood for at least 24 h to let the solvent evaporate.

For characterization, the fibrous scaffolds were sputter-coated with gold/palladium and visualized with a Cold Field Emission Scanning Electron Microscope (SEM, Hitachi SU8230, Japan). SEM images were analyzed using NIH ImageJ software. Average fiber diameter and fiber orientation were calculated for 300 fibers randomly picked from three different samples (Kuroda et al., 2014).

2.2. Human pluripotent stem cell culture and cardiac differentiation

Human induced pluripotent stem cells (IMR-90 (Yu et al., 2007)) were initially cultured on mouse embryonic fibroblast (MEF) feeders in hPSC medium and then expanded using either MEF-conditioned hPSC medium supplemented with 8 ng/mL human basic fibroblast growth factor (bFGF) or Essential 8™ (E8) medium on plates coated with growth factor-reduced Matrigel™ (1:60, *v*/*v*, cat No. CB-40230C, Fisher Scientific) (Bhagwati et al., 2013; Chen et al., 2011). hPSC medium was prepared using KnockOut DMEM medium supplemented with 20% (*v*/*v*) KnockOut serum replacement, 0.5 mM L-glutamine, 0.1 mM nonessential amino acids, 0.1 mM beta-mercaptoethanol, 1% (*v*/*v*) PenStrep (10,000 IU/mL penicillin,

10,000 μg/mL streptomycin solution), and 4 ng/mL bFGF. All culture media and reagents were purchased from Life Technologies unless otherwise specified. All cultures were maintained under standard culture conditions (5% CO_2, 37 °C).

Directed CM differentiation was achieved by a serial application of either growth factors (activin A and BMP4, R&D Systems) or small molecules (CHIR99021 and Wnt-C59, SelleckChem) under serum-free, monolayer culture conditions with minor modifications (Fig. S1) (Burridge et al., 2014; Laflamme et al., 2007). In brief, for growth factor-guided method, confluent undifferentiated hPSCs maintained in condition medium were dissociated with Versene for 5–7 min at 37 °C and then replated onto Matrigel-coated plates at 2×10^5 cells/cm^2. These cells were fed daily for 2 days with MEF-conditioned medium supplemented with 8 ng/mL bFGF. Once confluent, cells were treated with activin A at 100 ng/mL for 24 h (day 0) followed by 10 ng/mL BMP4 in serum-free Roswell Park Memorial Institute (RPMI) 1640 medium supplemented with insulin-free B27 for 4 days without medium change. Thereafter the cells were fed with RPMI medium with B27 containing insulin every other day. Cells were harvested at differentiation day 16–20 and CMs were enriched using Percoll gradient centrifugation method (Supplementary method) when the culture contained <70% CMs.

CM differentiation was also achieved using small molecules that target the Wnt pathways (Fig. S1) (Burridge et al., 2014). Briefly, confluent undifferentiated hPSCs maintained in E8 medium were dissociated with Versene for 5–7 min at 37 °C and then replated onto Matrigel-coated plates at 2.5×10^4 cells/cm^2. After being fed daily for 4 days with E8 medium, the near-confluent (>85% confluence) cultures were treated with CHIR99021 at 6 μM in serum-free medium RPMI supplemented with insulin-free B27 for 48 h followed by medium change. On day 3, the cultures were treated with 2 μM Wnt-C59 for another 48 h in RPMI/insulin-free B27. Starting from day 5, cells were maintained in the serum-free medium RPMI/B27 containing insulin and the medium was changed every other day.

2.3. Culture of hPSC-CMs on substrates

Electrospun fibrous scaffolds were sterilized by exposing both sides to a conventional ultraviolet (Chuva de Sousa Lopes et al.) source (30 W, 65 cm working distance) for 30 min each side in a laminar flow hood and were secured in 24-well culture plates using Viton O-rings (Size 014, cat No. LG-1022-510, Wilmad-LabGlass) (Ben-David et al., 2013). After coating at 4 °C for at least 8 h with 0.5 mL/well of growth factor reduced Matrigel (1:60, *v*/*v*), all samples were seeded with CMs (>70%) at a density of 7.5×10^5/cm^2 and maintained in RPMI/B27 medium for another 2 weeks. The culture medium was replenished every other day afterwards. After 2-week culturing on electrospun fibrous scaffolds or TCPs, the cells were either directly fixed for immunocytchemical analysis of cell alignment or harvested for RT-PCR analysis. For other analyses on cellular structure and functional features, cells were dissociated with 0.25% Trypsin/EDTA and replated to facilitate imaging and recordings.

2.4. Immunocytochemistry and imaging analyses

After 2-week culturing, cells dissociated were replated at 150 × 10^3/cm^2 on Matrigel-coated 96 well plates for cellular structure/feature analysis. All samples were fixed with freshly prepared 4% (*v*/*v*) paraformaldehyde (PFA, Sigma-Aldrich) for 15 min at room temperature (RT). For consistency, replated cells were fixed 48 h post-seeding. Upon permeabilization with 100% ice-cold ethanol (Sigma) for 2 min, the cells were blocked with 5% (*v*/*v*) normal goat serum (NGS) in PBS for 2 h at RT followed by incubation with primary antibodies (Abs) at optimal concentrations in 1% (*v*/*v*) NGS for overnight at 4 °C (Table S1). The cells were then washed twice in PBS for 5 min and incubated with secondary Abs at optimal concentrations (Table S1) for 1 h in the dark. After washing three times with PBS for 5 min each, cell-scaffold constructs were then mounted in VECTASHIELD® mounting medium with DAPI (Vector Laboratories Inc.) for confocal imaging. For replated cells, nuclei were counterstained with 1 μg/mL bisBenzimide Hoechst 33258 (cat No. B2883, Sigma-Aldrich) at RT for 15 min and then mounted with “GLOX” buffer (anti-fade buffer and enzymes) (Nori et al., 2015). Negative controls were carried out in parallel omitting the primary antibody.

Epifluorescence imaging was performed using a Zeiss inverted microscope equipped with appropriate optical filters. Digital images were acquired with a Zeiss AxioCam digital camera system and processed using Zeiss AxioVision LE imaging software. Images were analyzed with Adobe Photoshop (Adobe Systems). Cell size, shape, and sarcomere length were quantified using NIH ImageJ software. To visualize CM alignment in the cell-scaffold constructs, immunostaining of α-actinin was carried out and images were acquired using an inverted confocal scanning microscope (Olympus Fluoview 1000) equipped with FluoView software (Olympus). Confocal images in Z-stacks were projected with max intensity.

2.5. Real time quantitative RT-PCR

Total RNA was isolated from cells after they were cultured on fibrous scaffolds or TCPs for 2 weeks using an Aurum Total RNA mini kit (cat No. 732-6820, Bio-Rad); the genomic DNA was digested with RNase-free DNase provided in the kit, according to the manufacturer's instruction. The quality and quantity of the extracted RNA were analyzed on a Nanodrop spectrophotometer (ND-1000, Thermo Fisher Scientific). Total RNA (0.5 μg) was reverse-transcribed using a SuperScript® VILO™ cDNA kit (Life Technologies) per manufacturer's recommendation. Real-time PCR was performed in a 15 μL reaction mixture containing 1.5 μL of cDNA, 5.4 μL of nuclease-free water (Applied Biosystems), 200 nM of forward and reverse primers (Table S2) for each gene, and 2× iTaq™ SyBr Green master mix (cat No: 172-5124, Bio-Rad) and detected with an ABI 7500 RT PCR system(Applied Biosystems). A comparative Ct method was used for analyzing the level of each targeting gene, which was normalized to the Ct value of housekeeping gene glyceraldehyde 3-phosphate dehydrogenase (GAPDH). Fold of change was then calculated as $2^{-\Delta\Delta Ct}$.

2.6. Multielectrode array recordings

A multielectrode array (MEA) mapping data acquisition system (Axion Biosystems) was used to assess the electrophysiological phenotypes and pharmacological responses of CMs. Briefly, following enzymatic dissociation, cells were replated onto fibronectin-coated MEA

chambers at 3×10^5 cells per chamber and maintained in RPMI/B27 medium for 3–7 days prior to recording. Extracellular recordings were acquired using a 64-channel Muse MEA system (Axion Biosystems) for 30 s at baseline and after 5min upon incubation with each cardio-active pharmacological compound at ascending concentrations. Data were analyzed using the Axion's Integrated Studio software. Information about the compounds, their sources and concentrations is included in Table S3.

2.7. Calcium imaging

Live cell imaging was used to evaluate intracellular calcium transients. Briefly, cells were replated on Matrigel-coated glass coverslips for additional 3–7 days. Cells on glass coverslips were then incubated with 5 μM calcium indicator dye Fluo-4 AM (cat No. F14201, Life Technologies) and 2 drops/mL NucBlue® Live ReadyProbes® Reagent (Hoechst 33342, cat No. R37605, Life Technologies) at 37 °C for 15 min. After that, the glass coverslips were transferred to a temperature-controlled microscope chamber, and perfused with normal Tyrode's solution which was freshly prepared in ultrapure water (18 $M\Omega\ cm^{-1}$) containing 148.8 mM NaCl, 4 mM KCl, 0.53 mM $MgCl_2$, 1.8 mM $CaCl_2$, 0.33 mM NaH_2PO_4, 5 mM HEPES, and 5 mM D-glucose (pH adjusted to 7.4 with NaOH) (Nguyen et al., 2014; Tano et al., 2014). Optical recordings of intracellular calcium transients were acquired in line scan mode using an inverted confocal scanning microscope (Olympus Fluoview 1000) equipped with FluoView software (Olympus). The optical recordings were then analyzed with the Clampfit data analysis module of Axon™ pCLAMP™ 10 Electrophysiology data acquisition and analysis software (Molecular Devices).

2.8. Statistics

Data are expressed as mean± standard error (SE) when applicable. Sample size for each analysis is described in figure legends. Mann–Whitney *U* test, one-way or two-way ANOVA test was used where appropriate. The difference in the classification of sarcomeric organization was assessed using chi-square test. A *p*-value of 0.05 was considered significant.

3. Results

3.1. Preparation and characterization of electrospun fibrous scaffolds

To generate electrospun fibrous scaffolds that induce the anisotropic and isotropic CM alignment, we first prepared and characterized the aligned and random PCL fibrous meshes. As expected, electrospinning of PCL solution yielded bead-free and uniform fibers with distinct orientations (Fig. 1A). Histogram analysis of fiber alignment in each type of fibrous scaffolds confirmed the well-defined anisotropic and isotropic features (Fig. 1B). Fiber diameters showed a similar distribution in size in the range of 230–2200 nm, with an almost identical histogram peak frequency at 500–600 nm (Fig. 1C). As anticipated, the average sizes of aligned and random fibers were indistinguishable, and were at approximately 0.7 μm ($p > 0.05$, inset in Fig. 1C).

3.2. Culture of hPSC-CMs on electrospun fibrous scaffolds

To determine the effect of the electrospun fibrous scaffold culture on hSPC-CMs, we first prepared enriched CMs from batches of hPSCs containing approximately 98% of cells positive for stem cell markers SSEA-4 and TRA-1-60 (Fig. S1B). At the end of differentiation, cultures induced by growth factors contained up to approximately 70% CMs (Movie S1 and Fig. S1C), and cultures that had <70% purity were further enriched using Percoll gradient centrifugation to as high as 95% CMs (Fig. S1D). Cultures induced by small molecules contained >85% CMs (Movie S2 and Fig. S1E).

These hPSC-CMs (>70% purity) were then replated onto Matrigel-coated fibrous scaffolds and TCPs, and maintained for another 2 weeks (Fig. 2A). Often upon overnight culturing, the replated hPSC-CMs restarted spontaneous contractions. After 2 weeks growth, hPSC-CMs were stained with sarcomeric protein α-actinin, for the visualization of CMs within fibrous scaffolds. As shown in Fig. 2B, hPSC-CMs displayed distinct cellular organizations: CMs on aligned fibrous scaffolds were extended and elongated in the direction parallel to the fiber alignment whereas cells on random fibrous scaffolds stayed together and remained relatively circular, illustrating an apparent anisotropic or isotropic feature of CMs grown on the two different types of scaffolds. In comparison, cells cultured on TCPs formed large cellular bundles with random orientations (Fig. 2B, and Movie S3). These data confirmed the anisotropic alignment of hPSC-CMs induced by aligned PCL fibrous scaffolds.

3.3. Cardiac protein expression and structural characteristics

We replated the ensuing hPSC-CMs on Matrigel-coated plates and evaluated the structure characteristics by immunocytochemistry. All cardiac-relevant markers examined were detected on hPSC-CMs with little difference among cells on all substrates. In particular, the majority of the cells expressed sarcomeric proteins troponin T, myosin heavy chain (MHC), α-actinin, troponin I, cell adherens junction protein cadherin, as well as cardiac transcription factor NKX2.5 (Fig. 3). MLC-2A, a major myosin light chain (MLC) isoform that is expressed in both atria and ventricle, was detected in most cells (Fig. 3, row 4). MLC2V, another major MLC isoform that becomes restricted to ventricle at the late stage of development (de Chuva et al., 2006) and has been used to indicate maturity of ventricular CMs (Lian et al., 2012), was only detected in a small number of cells (Fig. 3, row 4). The observation on MLC-2A and MLC-2V is consistent with a previous report for differentiation day 30 hPSC-CMs (Burridge et al., 2014) and indicates a fetal-like cell phenotype. On the other hand, smooth muscle actin, a marker known to label immature CMs and be replaced by skeletal actin and cardiac actin as development proceeds (Clement et al., 2007), was only detected in a small number of cells (Fig. 3, row 1). Ki67, a cell proliferation indicator, was also only detected in a small number of cells (Fig. 3, row 5, arrows), suggesting that the cells on all substrates were of low proliferative capabilities. Altogether, the immunochemical analyses indicate that the hPSC-CMs cultured on all substrates expressed CM-associated proteins although likely with an immature phenotype.

To assess the structural maturation of the hPSC-CMs, we analyzed the levels of the organization of the Z-line protein α-actinin as well as CM morphology. In particular, the extent of sarcomeric striation on hPSC-CMs was evaluated and categorized into four

different levels (Birket et al., 2013; Nguyen et al., 2014; Ribeiro et al., 2015): Level I cells were α-actinin$^+$ but without clear sarcomeric striations; Level II displayed some striations but largely with dotted structure; Level III showed patterned striations in more than half but not nearly the whole cell area; Level IV exhibited high sarcomeric organization with distinct paralleled bands in almost the whole cell area (Fig. 4A). The hPSC-CMs on the aligned fibrous scaffolds exhibited significantly improved levels of sarcomeric organization, comparing with those on the TCPs ($p < 0.05$, Fig. 4B). Particularly, those cells exhibited the highest proportions of cells in levels III and IV, reaching a total of 75%, comparing to 63% as detected on TCPs (Fig. 4B). In terms of cell size, hPSC-CMs cultured on the aligned fibrous scaffolds were significantly larger than those on the random ones (864 ± 37 μm^2 versus 745 ± 37 μm^2, $p < 0.05$, Fig. 4C, left), and cells on the two fibrous scaffolds were significantly smaller, compared with those on the TCPs (1053 ± 52 μm^2, $p < 0.05$, Fig. 4C, left). In addition, hPSC-CMs on the aligned fibrous scaffolds were significantly more elongated than those on the random (circularity 0.43 ± 0.01 versus 0.48 ± 0.01, $p < 0.05$, Fig. 4C, right). Additionally, analysis of the sarcomere length of level IV cells revealed no significant difference among all substrates (sarcomere length c.a. 1.4 μm, $p > 0.05$, Fig. 4C). Collectively, these data suggest that hPSC-CMs cultured on the aligned fibrous scaffolds displayed a slightly more mature structure than those on the random but not sufficiently more structurally mature than cells on TCPs.

3.4. Cardiac gene expression

To examine the expression of CM-associated genes, we performed qRT-PCR on cells grown on the three substrates. This analysis detected genes encoding structural proteins such as troponin T type 2 (*TNNT2*), troponin I type 3 (*TNNI3*), myosin light chain 7 (*MYL7*, also known as MLC-2A), myosin heavy chain 6 (*MYH6*, also known as α-MHC), myosin heavy chain 7 (*MYH7*, or β-MHC), the Z-disc and M-line anchor protein titin (*TTN*) (Fig. 5A) as well as ion channels or calcium handling proteins such as sarco/endoplasmic reticulum Ca^{2+} ATPase (*ATP2A2* or *SERCA2*), calsequestrin 2 (*CASQ2*), hyperpolarization activated cyclic nucleotide-gated potassium channel 1 (*HCN1*), potassium inwardly rectifying Kir2.1 channel (*KCNJ2*), voltage-gated potassium Kv1.4 channel (*KCNA4*), and Na^+-Ca^{2+} exchanger (*SLC8A1* or *NCX1*) (Fig. 5B). Among the 13 genes, 9 of them including *TNNT2*, *MYL7*, *MYH6*, and *TTN* that encode structural proteins (1.9–2.4 folds, $p < 0.05$, Fig. 5A) and *ATP2A2*, *CASQ2*, *HCN1*, *KCNJ2* and *KCNA4* that encode ion channels or calcium handing proteins (1.8–2.8 fold, $p < 0.05$, Fig. 5B) were detected at higher expression levels in cells on the aligned fibrous scaffolds than those on TCP. In addition, expression levels of 6 genes (*MYH6*, *TTN*, *CASQ2*, *HCN1*, *KCNJ2* and *KCNA4*) were significantly increased in cells on random fibrous scaffolds compared to those on the TCPs ($p < 0.05$, Fig. 5). In contrast, only 2 genes (*CASQ2* and *KCNJ2*) were significantly upregulated in cells on the aligned fibrous scaffolds compared to those on the random fibers ($p < 0.05$, Fig. 5). Together, these data show that the expression of several CM-associated genes in hPSC-CMs on aligned or random electrospun fibrous scaffolds significantly increased compared with cells on TCPs; however, cells on aligned fibrous scaffolds and random fibrous scaffolds had similar levels of expression for the majority of genes examined.

3.5. Evaluation of pharmacological responses

To assess the pharmacological responses of the ensuing hPSC-CMs, we treated the cells with several cardio-active compounds, including α- or β- adrenergic receptor agonist, muscarinic agonist, and gap junction uncoupler, and then evaluated the chronotropic responses (changes in the beating frequency) (Table S3). In these studies, hPSC-CMs from cultures on all substrates positively responded to isoproterenol (a β-adrenergic receptor agonist, up to 1.6–1.7 fold, Fig. 6A) and phenylephrine (an α-adrenergic receptor agonist, up to 1.4–1.5 fold, Fig. 6B), while negatively responded to carbamylcholine (a muscarinic agonist, up to 0.8–0.9 fold, Fig. 6C). In addition, upon the treatment with a gap junction uncoupler heptanol, hPSC-CMs from cultures on all three substrates displayed undetectable electrical activation (Fig. 6D). These observations indicate that the α- and β-adrenergic receptors, muscarinic receptors, and gap junction proteins were appropriately expressed on cells cultured on all substrates. Moreover, hPSC-CMs responded to each of these drugs similarly among three substrates ($p > 0.05$, by two-way ANOVA *post hoc* Tukey test) (Fig. 6). Overall, these data indicate that hPSC-CMs from cultures on all three substrates exhibited appropriate pharmacological responses to α- and β-adrenergic and muscarinic receptor agonists as well as a gap junctional uncoupler yet without significant differences among cells on all three substrates.

3.6. Assessment of intracellular calcium transients

To evaluate the calcium handling properties, we replated the ensuing hPSC-CMs onto Matrigel-coated glass coverslips, and assessed their intracellular calcium transients. Line-scan of the time-lapse spontaneous calcium transient of CMs was performed and the intracellular calcium transient was recorded (Fig. 7A–C). As illustrated in Fig. 7D, the average beating rates of cells from cultures on the two fibers were significantly lower (19 ± 10 bpm for aligned fibers, 22 ± 14 bpm for random fibers) than those on the TCPs (29 ± 1 bpm, $p < 0.05$,). And the times to 50% peak and 50% decay of hPSC-CMs from cultures on the two fibers were significantly longer than cells on TCPs ($p < 0.05$, Fig. 7D). In contrast, no statistically significant difference was observed in the peak amplitude among cells on all three substrates (Fig. 7D). These data indicate that hPSC-CMs from cultures on all three substrates exhibited CM-specific calcium handling properties, albeit prolonged calcium transient duration and slower beating rates were observed in cells on the two types of fibrous scaffolds, suggesting not necessarily enhanced cell maturation.

4. Discussion

The generation of bona fide mature hPSC-CMs is required for accurate and robust disease modeling and drug screening. To this end, increasing efforts have been applied to improve the maturation of hPSC-CMs using various methods. Cell alignment has been suggested as one of the approaches to improve the maturation of hPSC-CM. However, it was unclear if cell alignment alone was sufficient to enhance robust maturation of hPSC-CMs. In this study, we synthesized submicron fibrous scaffolds with aligned or random orientations, and investigated the effect of these scaffolds on the cell alignment and maturation of hPSC-CMs. As anticipated, hPSC-CMs on aligned fibrous scaffolds preferentially elongated in the direction parallel to the fiber alignment. Compared with cells on TCPs, the hPSC-CMs on

aligned fibrous scaffolds had modest improvement on structural maturation, similar levels of CM-associated proteins and pharmacological responses, and increased levels of expression of several CM-associated genes. However, their calcium transient kinetics were slower than that of cells from cultures on TCPs, suggesting the limited effect of aligned fibrous scaffolds in improving the hPSC-CM maturation.

Comparing with cells on the TCPs, hPSC-CMs grown on the aligned fibrous scaffolds had enhanced molecular maturation. For instance, genes encoding ion channel or calcium handling proteins, such as *ATP2A2*/*SERCA2*, *CASQ2*, *HCN1*, *KCNJ2*, and *KCNA4*, were universally increased in cells on aligned fibrous scaffolds. Particularly, *CASQ2* and *KCNJ2*, encoding the most abundant, high-capacity but low-infinity Ca^{2+}-binding protein calsequestrin that stores and buffers Ca^{2+} in the sarcoplasmic reticulum (Liu et al., 2009) and potassium inwardly rectifying Kir2.1 channel, respectively, were also significantly upregulated when compared to the random. These upregulations are consistent with the reported observations for hPSC-CMs subjected to prolonged culture, electrical stimulation, mechanical stretch or 3-D tissue formation (Lieu et al., 2013; Lundy et al., 2013; Mihic et al., 2014; Tulloch et al., 2011; Zhang et al., 2013) which were shown to enhance CM maturation.

A higher proportion of hPSC-CMs on aligned fibrous scaffolds had increased levels of sarcomeric striations than cells on TCPs, albeit the average length of sarcomeres was similar and the average cell size of hPSC-CMs from cultures on the scaffolds was significantly smaller. The observation of reduced cell area for cells on the fibrous scaffolds is consistent with the published literatures (Bashur et al., 2006; Han et al., 2013), where reduced sizes of human aortic endothelial cells and 3T3 fibroblasts were observed in cells on the random electrospun fibrous scaffolds, comparing with those on the natural protein-coated glass coverslips or TCPs. It was reported that for substrata with uniform ridges and grooves, cells tended to reduce their sizes when they were on surfaces with either over-narrowed or over-wide scales, because of the limited cell penetration into over-narrowed grooves, or the loss of the extra cell-substratum contact on surfaces with the over-wide grooves (Kim et al., 2010). We surmise that our submicron electrospun fibers, in a 3-D scaffolding environment, may confine the penetration of the cells therefore reduced the cell spatial organization. Future studies with an optimal fiber size/scaffold topology which can be modulated by the electrospinning parameters (Kuroda et al., 2014) may increase the cell spreading and improve cell maturation (Han et al., 2013). In addition, a stage-specific and dynamic design of the fiber size/scaffold topology may be more beneficial, as the size of hPSC-CMs constantly enlarges during maturing.

The chronotropic responses of the hPSC-CMs to various cardioactive drugs in our study are well in line with the published results (Mandel et al., 2012; Pillekamp et al., 2009; Pillekamp et al., 2012; Xu et al., 2002), in which the beating rates of CMs were increased in response to isoproterenol and phenylephrine, and decreased in response to carbamylcholine. While the pharmacological responsiveness of the cells was similar, the calcium cycling of hPSC-CMs from cultures on the two types of fibrous scaffolds were significantly prolonged. Lundy et al. found that late stage hPSC-CMs (differentiation day 80+) exhibited faster spontaneous Ca^{2+} transient kinetics, i.e., significant reduction in time to peak and time to 50% decay,

while the transient peak amplitude remained unchanged, comparing with early stage cells (differentiation day 20–40) (Lundy et al., 2013). Similarly, we found statistically unchanged peak amplitude in spontaneous Ca^{2+} transients. However, the increases in 50% rise to peak time and peak to 50% decay time suggest unimproved maturation for cells on fibrous scaffolds, comparing with cells on TCPs.

A potential limitation of our studies is that some of the analyses were conducted after the cells were lifted from fibrous scaffolds with trypsin, replated onto Matrigel-coated surface, and then cultured in the absence of topographic cues for a few days. Although the experimental design was to facilitate imaging and recordings for the analyses of the effect of fibrous scaffolds on the maturation of hPSC-CMs, replating could have disrupted the nascent extracellular matrix and cell–cell contacts, and the removal of topographic features could have affected the resultant morphological, biochemical and functional properties of hPSC-CMs.

There are several challenges and considerations in promoting the maturation of hPSC-CMs in vitro. First, hPSC-CMs are dramatically different from human adult ventricular cardiomyocytes. For example, human adult ventricular cardiomyocytes in culture have a surface area of approximately 12,000 μm^2 (Li et al., 1996), which is at least 11 fold larger than hPSC-CMs examined in the current study, and the sarcomere length of relaxed human cardiac muscle cell is approximately 2.2 μm (Bird et al., 2003), which is about 1.5 fold of the value in hPSC-CMs observed in this study. In vivo, it can take 6–7 years for human CMs to reach certain features of adult CMs (Peters et al., 1994), suggesting the necessity of expedited maturation for hPSC-CMs differentiated in vitro. Second, most studies to date including our present study used hPSC-CM population with heterogeneous maturation levels of immature embryonic or neonatal-like CMs, as reflected in different levels of maturation in sarcomeric organizations and electrophysiological properties (Veerman et al., 2015; Yang et al., 2014). Third, the hPSC-CMs generated so far are mixed populations of nodal-, atrial-, or ventricular-like cells (Veerman et al., 2015; Yang et al., 2014). Distinct profiles in their gene expression as well as the electrophysiological properties will undoubtedly lead inaccurate evaluation in CM maturation. Yet with subtype specification, we can precisely gauge and evaluate the maturation stage of hPSC-CMs, which in turn, will contribute to the homogeneity of the cell maturation. Forth, the molecular, structural, and functional phenotypes of CMs change constantly during development. Thus using stage-specific human CMs, like the fetal, neonatal, postnatal, or adult CMs as the references to gauge the maturation level, will provide a more accurate characterization (Ribeiro et al., 2015). Last but not the least, in native 3-D cardiac environment, the underlying ECM, the neighboring non-CMs, together with the surrounding biochemical, mechanical, and electrical signals act synergistically to modulate the maturation of CMs (Ma et al., 2014; Veerman et al., 2015; Yang et al., 2014). Combinatorial methods by applying 3-D culturing with electrical stimulation, mechanical stretch and co-culture with vascular cells, or microgroove alignment and biochemical treatment, have thus far achieved promising results (Nunes et al., 2013; Ribeiro et al., 2015; Tulloch et al., 2011). Therefore, the enhanced and expedited maturation of hPSC-CMs may be significantly advanced by addressing the present challenges in CM purification (subtype specification/differentiation), heterogeneity and variability in cell

maturity, using the stage-relevant human CMs as the references, as well as the combinatorial use of multiple microenvironment factors.

5. Conclusions

We show that using a physiologically relevant aligned fibrous scaffold as a single approach has limited ability in improving the maturation of hPSC-CMs. Nevertheless, this work provides a proof-of-concept for the use of electrospun aligned fibrous scaffold in inducing efficient alignment of hPSC-CMs and highlights the need for a combination of the cell alignment with other methods to create physiologically relevant microenvironment for improving the maturation of hPSC-CMs.

Supplementary Material

Refer to Web version on PubMed Central for supplementary material.

Acknowledgments

We thank Dr. Wenying Liu for her help with the initial setup of the electrospinning and Mr. Xiyu Li for his assistance with SEM. We also thank Emory Children's Pediatric Research Center Flow Cytometry Core and Animal Physiology Core, which are supported by Children's Healthcare of Atlanta. Q.W. was supported by the Center for Pediatric Nanomedicine at Emory/Georgia Tech. This project was supported in part by the NIH grants R21HL118454 and R21HL123928 to C.X.

Abbreviations

3-D	three-dimensional
bFGF	human basic fibroblast growth factor
BMP4	bone morphogenetic protein 4
CM	cardiomyocyte
ECM	extracellular matrix
GAPDH	glyceraldehyde 3-phosphate dehydrogenase
hPSC	human pluripotent stem cell
MEF	mouse embryonic fibroblast
MEA	multielectrode array
MHC	myosin heavy chain
MLC	myosin light chain
NGS	normal goat serum
PFA	paraformaldehyde
PCL	polycaprolactone

PU	polyurethane
RPMI	Roswell Park Memorial Institute 1640 medium
RT	room temperature
SE	standard error
SEM	scanning electron microscope
TCP	tissue culture polystyrene

References

Barnes CP, et al. Nanofiber technology: designing the next generation of tissue engineering scaffolds. Adv. Drug Deliv. Rev. 2007; 59:1413–1433. [PubMed: 17916396]

Bashur CA, et al. Effect of fiber diameter and orientation on fibroblast morphology and proliferation on electrospun poly (d,l-lactic-co-glycolic acid) meshes. Biomaterials. 2006; 27:5681–5688. [PubMed: 16914196]

Ben-David U, et al. Immunologic and chemical targeting of the tight-junction protein Claudin-6 eliminates tumorigenic human pluripotent stem cells. Nat. Commun. 2013; 4:1992. [PubMed: 23778593]

Bhagwati C, et al. Profile of the Chikungunya infection: a neglected vector borne disease which is prevalent in the Rajkot District. J. Clin. Diagn. Res. 2013; 7:1008–1011. [PubMed: 23905091]

Bird SD, et al. The human adult cardiomyocyte phenotype. Cardiovasc. Res. 2003; 58:423–434. [PubMed: 12757876]

Birket MJ, et al. PGC-1alpha and reactive oxygen species regulate human embryonic stem cell-derived cardiomyocyte function. Stem Cell Rep. 2013; 1:560–574.

Burridge PW, et al. Production of de novo cardiomyocytes: human pluripotent stem cell differentiation and direct reprogramming. Cell Stem Cell. 2012; 10:16–28. [PubMed: 22226352]

Burridge PW, et al. Chemically defined generation of human cardiomyocytes. Nat. Methods. 2014; 11:855–860. [PubMed: 24930130]

Chen G, et al. Chemically defined conditions for human iPSC derivation and culture. Nat. Methods. 2011; 8:424–429. [PubMed: 21478862]

Chen A, et al. Integrated platform for functional monitoring of biomimetic heart sheets derived from human pluripotent stem cells. Biomaterials. 2014; 35:675–683. [PubMed: 24144905]

Cipitria A, Skelton A, Dargaville TR, Dalton PD, Hutmacher DW. Design, fabrication and characterization of PCL electrospun scaffolds—a review. J. Mater. Chem. 2011; 21:9419–9453.

Clement S, et al. Expression and function of alpha-smooth muscle actin during embryonic-stem-cell-derived cardiomyocyte differentiation. J. Cell Sci. 2007; 120:229–238. [PubMed: 17179203]

Chuva de Sousa Lopes SM, et al. Patterning the heart, a template for human cardiomyocyte development. Dev. Dyn. 2006; 235:1994–2002. [PubMed: 16649168]

Han J, et al. Tissue factor activity and ECM-related gene expression in human aortic endothelial cells grown on electrospun biohybrid scaffolds. Biomacromolecules. 2013; 14:1338–1348. [PubMed: 23560456]

Kamakura T, et al. Ultrastructural maturation of human-induced pluripotent stem cell-derived cardiomyocytes in a long-term culture. Circ. J. 2013; 77:1307–1314. [PubMed: 23400258]

Khan M, et al. Evaluation of changes in morphology and function of human induced pluripotent stem cell derived cardiomyocytes (HiPSC-CMs) cultured on an aligned-nanofiber cardiac patch. PLoS One. 2015; 10:e0126338. [PubMed: 25993466]

Kim DH, et al. Nanoscale cues regulate the structure and function of macroscopic cardiac tissue constructs. Proc. Natl. Acad. Sci. U. S. A. 2010; 107:565–570. [PubMed: 20018748]

Kuroda T, et al. In vitro detection of residual undifferentiated cells in retinal pigment epithelial cells derived from human induced pluripotent stem cells. Methods Mol. Biol. 2014; 1210:183–192. [PubMed: 25173169]

Laflamme MA, et al. Cardiomyocytes derived from human embryonic stem cells in pro-survival factors enhance function of infarcted rat hearts. Nat. Biotechnol. 2007; 25:1015–1024. [PubMed: 17721512]

Li RK, et al. Human pediatric and adult ventricular cardiomyocytes in culture: assessment of phenotypic changes with passaging. Cardiovasc. Res. 1996; 32:362–373. [PubMed: 8796124]

Li WJ, et al. Electrospun nanofibrous structure: a novel scaffold for tissue engineering. J. Biomed. Mater. Res. 2002; 60:613–621. [PubMed: 11948520]

Lian X, et al. Robust cardiomyocyte differentiation from human pluripotent stem cells via temporal modulation of canonical Wnt signaling. Proc. Natl. Acad. Sci. U. S. A. 2012; 109:E1848–E1857. [PubMed: 22645348]

Liau B, et al. Pluripotent stem cell-derived cardiac tissue patch with advanced structure and function. Biomaterials. 2011; 32:9180–9187. [PubMed: 21906802]

Lieu DK, et al. Mechanism-based facilitated maturation of human pluripotent stem cell-derived cardiomyocytes. Circ. Arrhythm. Electrophysiol. 2013; 6:191–201. [PubMed: 23392582]

Liu J, et al. Facilitated maturation of Ca^{2+} handling properties of human embryonic stem cell-derived cardiomyocytes by calsequestrin expression. Am. J. Physiol. Cell Physiol. 2009; 297:C152–C159. [PubMed: 19357236]

Lundy SD, et al. Structural and functional maturation of cardiomyocytes derived from human pluripotent stem cells. Stem Cells Dev. 2013; 22:1991–2002. [PubMed: 23461462]

Ma Z, et al. Three-dimensional filamentous human diseased cardiac tissue model. Biomaterials. 2014; 35:1367–1377. [PubMed: 24268663]

Mandel Y, et al. Human embryonic and induced pluripotent stem cell-derived cardiomyocytes exhibit beat rate variability and power-law behavior. Circulation. 2012; 125:883–893. [PubMed: 22261196]

McCain ML, et al. Micromolded gelatin hydrogels for extended culture of engineered cardiac tissues. Biomaterials. 2014; 35:5462–5471. [PubMed: 24731714]

Mihic A, et al. The effect of cyclic stretch on maturation and 3D tissue formation of human embryonic stem cell-derived cardiomyocytes. Biomaterials. 2014; 35:2798–2808. [PubMed: 24424206]

Mummery CL, et al. Differentiation of human embryonic stem cells and induced pluripotent stem cells to cardiomyocytes: a methods overview. Circ. Res. 2012; 111:344–358. [PubMed: 22821908]

Nguyen DC, et al. Microscale generation of cardiospheres promotes robust enrichment of cardiomyocytes derived from human pluripotent stem cells. Stem Cell Rep. 2014; 3:260–268.

Nori S, et al. Long-term safety issues of iPSC-based cell therapy in a spinal cord injury model: oncogenic transformation with epithelial-mesenchymal transition. Stem Cell Rep. 2015; 4:360–373.

Nunes SS, et al. Biowire: a platform for maturation of human pluripotent stem cell-derived cardiomyocytes. Nat. Methods. 2013; 10:781–787. [PubMed: 23793239]

Peters NS, et al. Spatiotemporal relation between gap junctions and fascia adherens junctions during postnatal development of human ventricular myocardium. Circulation. 1994; 90:713–725. [PubMed: 8044940]

Pillekamp F, et al. Physiological differences between transplanted and host tissue cause functional decoupling after in vitro transplantation of human embryonic stem cell-derived cardiomyocytes. Cell. Physiol. Biochem. 2009; 23:65–74. [PubMed: 19255501]

Pillekamp F, et al. Contractile properties of early human embryonic stem cell-derived cardiomyocytes: beta-adrenergic stimulation induces positive chronotropy and lusitropy but not inotropy. Stem Cells Dev. 2012; 21:2111–2121. [PubMed: 22268955]

Radisic M, et al. Functional assembly of engineered myocardium by electrical stimulation of cardiac myocytes cultured on scaffolds. Proc. Natl. Acad. Sci. U. S. A. 2004; 101:18129–18134. [PubMed: 15604141]

Rao C, et al. The effect of microgrooved culture substrates on calcium cycling of cardiac myocytes derived from human induced pluripotent stem cells. Biomaterials. 2013; 34:2399–2411. [PubMed: 23261219]

Ribeiro MC, et al. Functional maturation of human pluripotent stem cell derived cardiomyocytes in vitro - correlation between contraction force and electrophysiology. Biomaterials. 2015; 51:138–150. [PubMed: 25771005]

Salick MR, et al. Micropattern width dependent sarcomere development in human ESC-derived cardiomyocytes. Biomaterials. 2014; 35:4454–4464. [PubMed: 24582552]

Senel Ayaz HG, et al. Textile-templated electrospun anisotropic scaffolds for regenerative cardiac tissue engineering. Biomaterials. 2014; 35:8540–8552. [PubMed: 25017096]

Tano K, et al. A novel in vitro method for detecting undifferentiated human pluripotent stem cells as impurities in cell therapy products using a highly efficient culture system. PLoS One. 2014; 9:e110496. [PubMed: 25347300]

Thavandiran N, et al. Design and formulation of functional pluripotent stem cell-derived cardiac microtissues. Proc. Natl. Acad. Sci. U. S. A. 2013; 110:E4698–E4707. [PubMed: 24255110]

Tulloch NL, et al. Growth of engineered human myocardium with mechanical loading and vascular coculture. Circ. Res. 2011; 109:47–59. [PubMed: 21597009]

Veerman CC, et al. Immaturity of human stem-cell-derived cardiomyocytes in culture: fatal flaw or soluble problem? Stem Cells Dev. 2015; 24:1035–1052. [PubMed: 25583389]

Xiao Y, et al. Microfabricated perfusable cardiac biowire: a platform that mimics native cardiac bundle. Lab Chip. 2014; 14:869–882. [PubMed: 24352498]

Xie J, et al. Conductive core-sheath nanofibers and their potential application in neural tissue engineering. Adv. Funct. Mater. 2009; 19:2312–2318. [PubMed: 19830261]

Xu C, et al. Characterization and enrichment of cardiomyocytes derived from human embryonic stem cells. Circ. Res. 2002; 91:501–508. [PubMed: 12242268]

Yang X, et al. Engineering adolescence: maturation of human pluripotent stem cell-derived cardiomyocytes. Circ. Res. 2014; 114:511–523. [PubMed: 24481842]

Yu J, et al. Induced pluripotent stem cell lines derived from human somatic cells. Science. 2007; 318:1917–1920. [PubMed: 18029452]

Zhang D, et al. Tissue-engineered cardiac patch for advanced functional maturation of human ESC-derived cardiomyocytes. Biomaterials. 2013; 34:5813–5820. [PubMed: 23642535]

Zhao S, et al. Nanofibrous patterns by direct electrospinning of nanofibers onto topographically structured non-conductive substrates. Nanoscale. 2013; 5:4993–5000. [PubMed: 23636504]

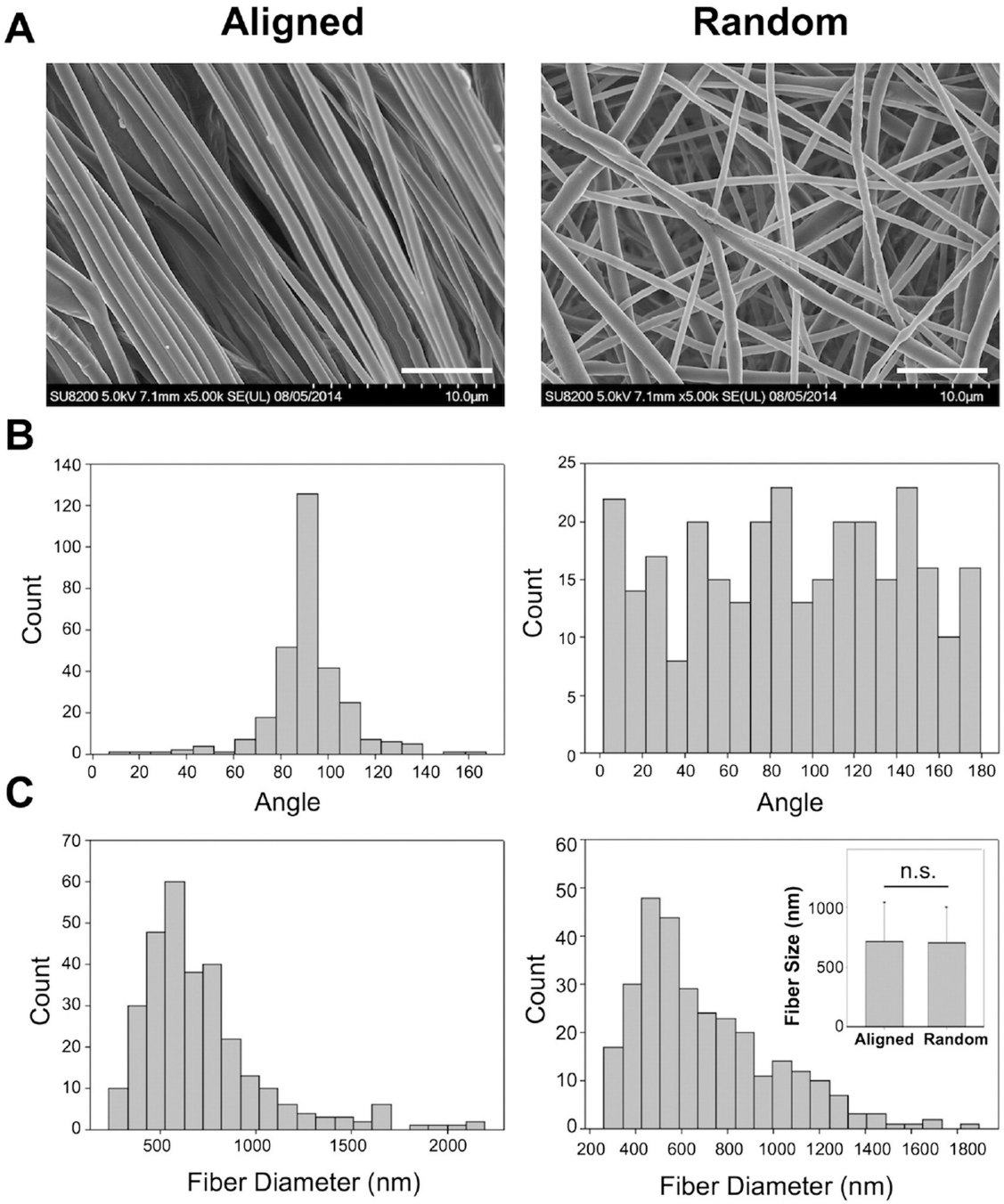

Fig. 1.

Aligned and random of electrospun PCL fibrous scaffolds. (A) SEM micrographs, (B) histograms of fiber orientations, and (C) histograms of fiber diameters of both aligned and random fibrous scaffolds. Inset in (C): the averaged fiber diameters of aligned and random fibrous scaffolds. Data were expressed as mean ± standard deviation (n = 300). n.s. not significant via Mann–Whitney *U* test. Scale bar in (A): 5 μm.

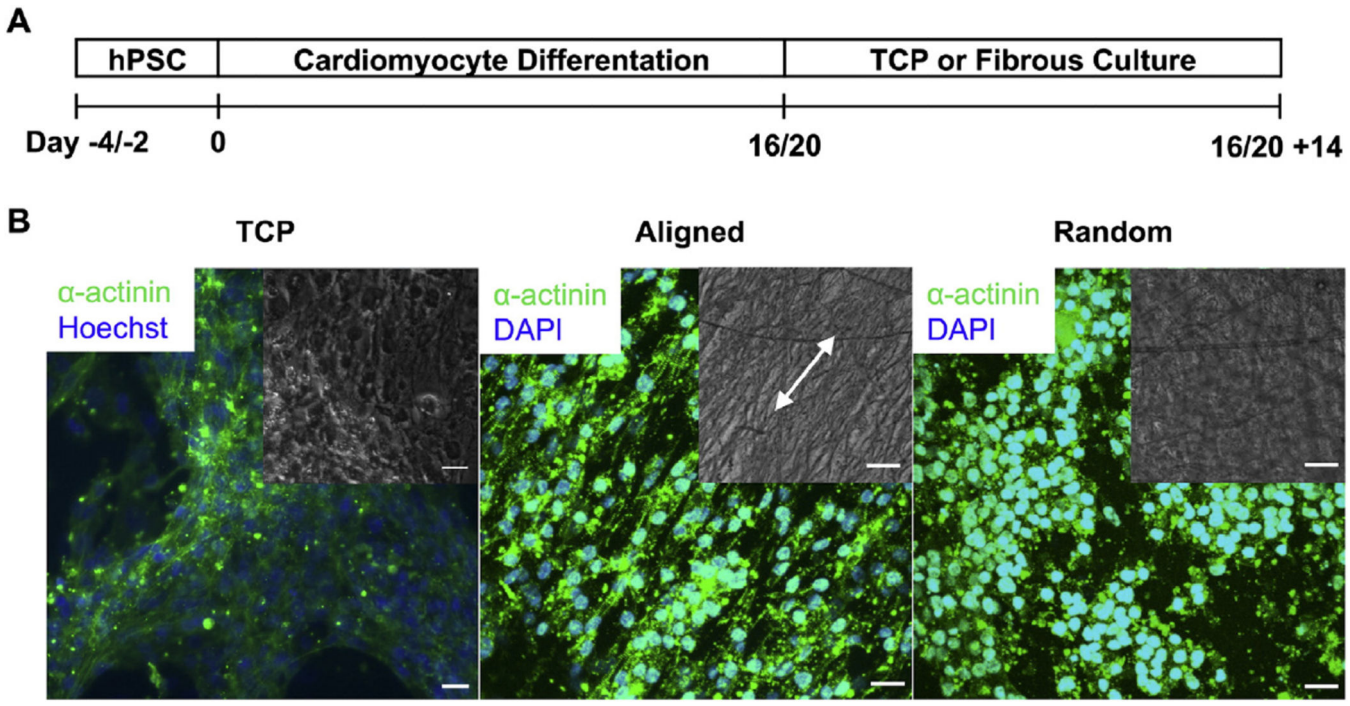

Fig. 2.

Anisotropic or isotropic alignment of hPSC-CMs cultured on the three substrates. (A) Schematic illustration of procedures used to directly differentiate hPSCs into CMs and to culture differentiated CMs on electrospun fibrous scaffolds or tissue culture polystyrenes (TCPs). After the cells were cultured on fibrous scaffolds or TCPs for 2 weeks, they were fixed directly and then subjected to immunocytochemical analysis of cell alignment. (B) Epi-/confocal-fluorescence micrographs of hPSC-CMs grown on various substrates for 14 days. Insets in (B): the corresponding phase-contrast images of hPSC-CMs cultured on various substrates. The white arrow indicated the alignment of fiber/cells. Scale bar: 20 μm.

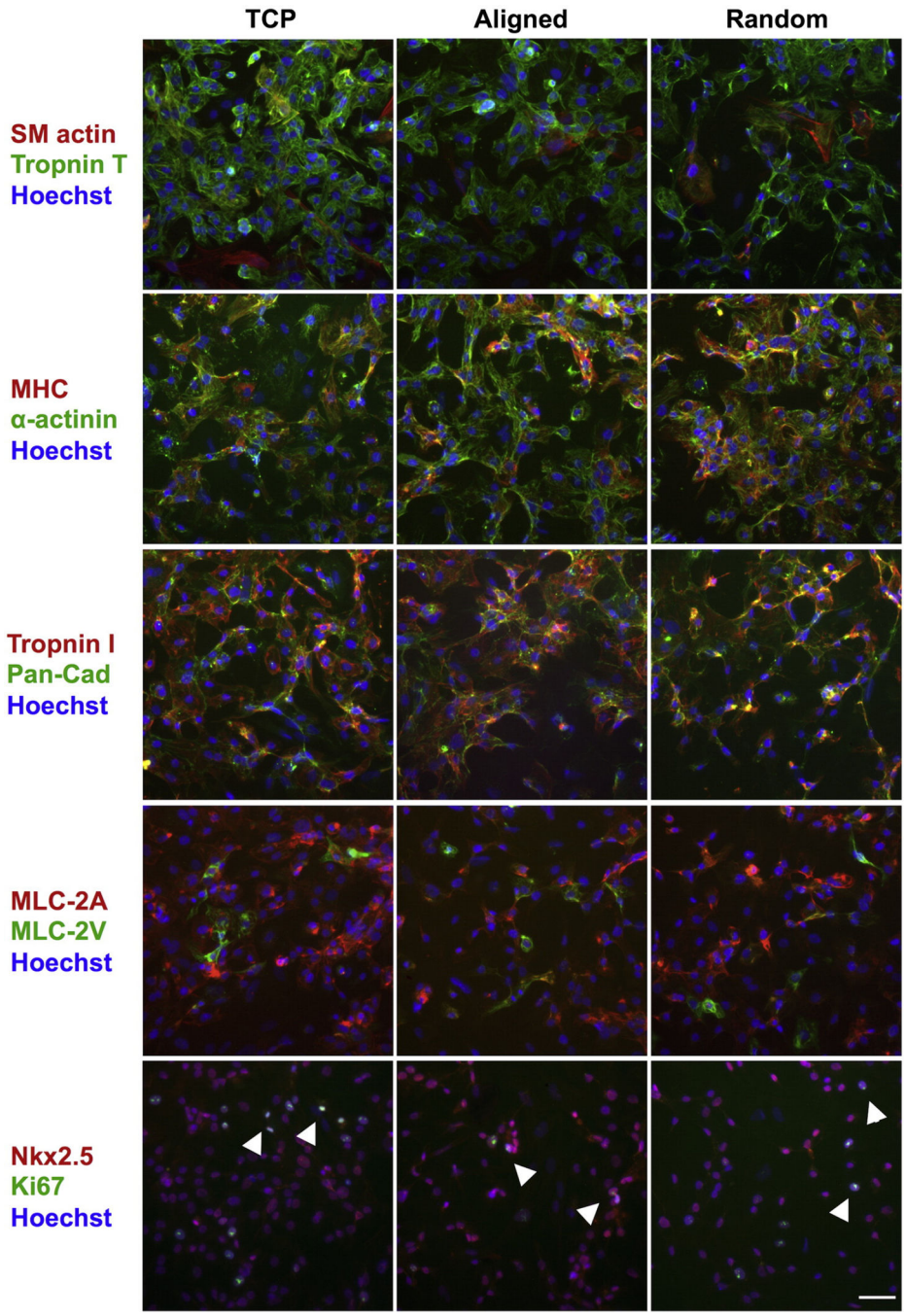

Fig. 3.

Immunocytochemical analysis of hPSC-CMs. Cells cultured on TCPs, aligned and random fibrous scaffolds for 2 weeks were harvested, replated onto 96-well culture plates, cultured for 48 h and stained with antibodies against smooth muscle actin (SM actin, red, row 1), troponin T (green, row 1), myosin heavy chain (MHC, red, row 2), α-actinin (green, row 2), troponin I (red, row 3), pan-cadherin (Pan-cad, green, row 3), myosin light chain 2A (red, row 4) and 2V (green, row 4), transcription factor NKX2.5 (red, row 5), Ki67 (green, row 5).

Cell nuclei were counterstained with Hoechst 33,258. Arrows in row 5 indicate the staining of Ki-67. Scale bar: 50 μm.

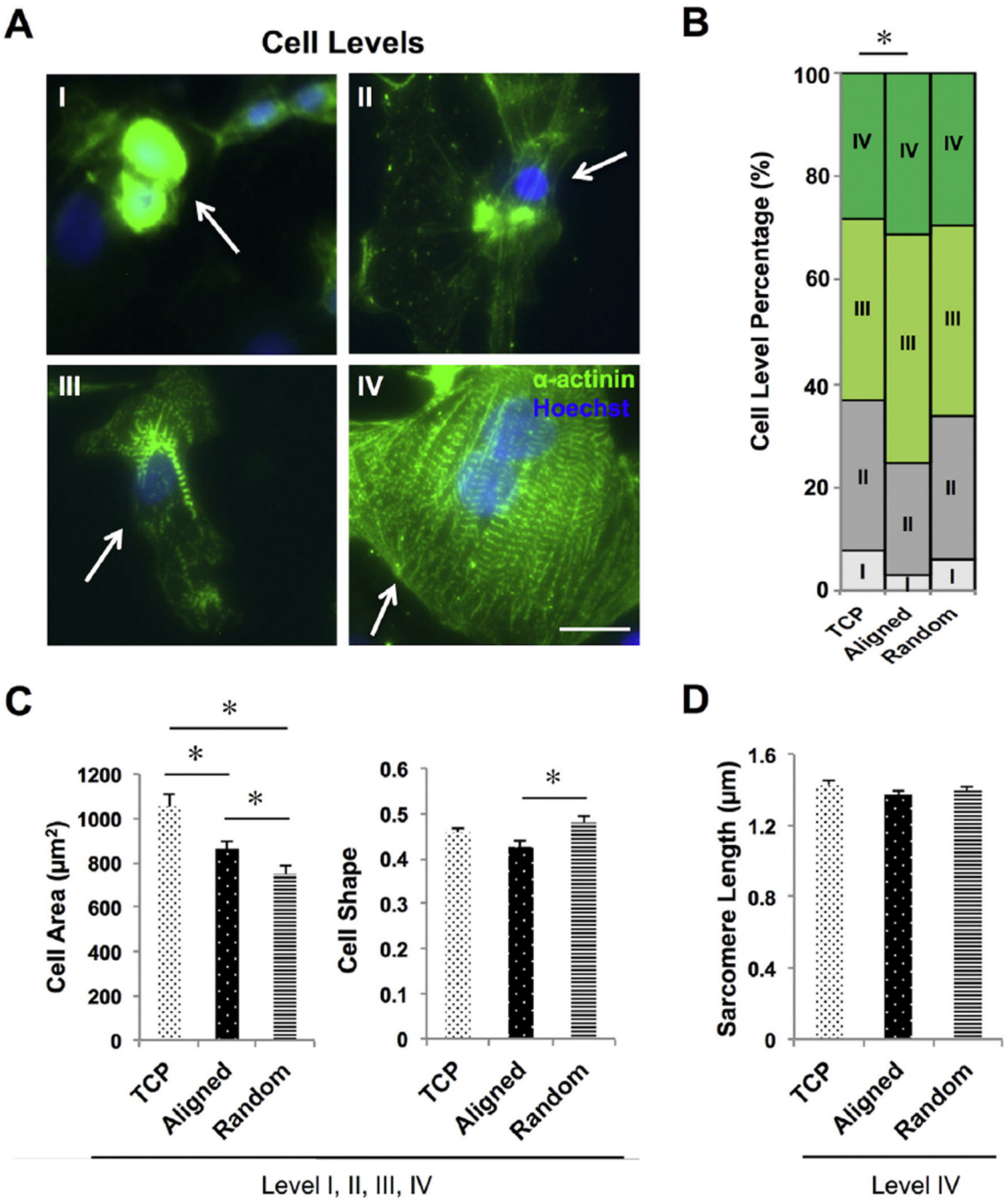

Fig. 4.

Structural characterization of hPSC-CMs. (A) Representative fluorescent images of hPSC-CMs (arrows) in different levels (I–IV), evaluated by their degrees of sarcomeric striations as indicated by α-actinin staining. Cells categorized in level I were α-actinin + but without clear sarcomeric striations, and cells in levels II, III, IV had detectable sarcomeric striations at increasing levels. Scale bar: 20 μm. (B) Percentages of cells categorized by their sarcomeric striation levels (n = 268–332). *: $p < 0.05$ via chi square test. (C) Quantification of cell size and shape in CMs of all levels (n = 268–332, circularity: 0 = line, 1 = circle), and

(D) sarcomere length of hPSC-CMs in level IV only (n = 79–103). Data represented cells from at least 10 random fields per experiment of three independent experiments. *: $p < 0.05$ via Kruskal–Wallis one-way ANOVA on ranks using Dunn's method for pairwise multiple comparisons.

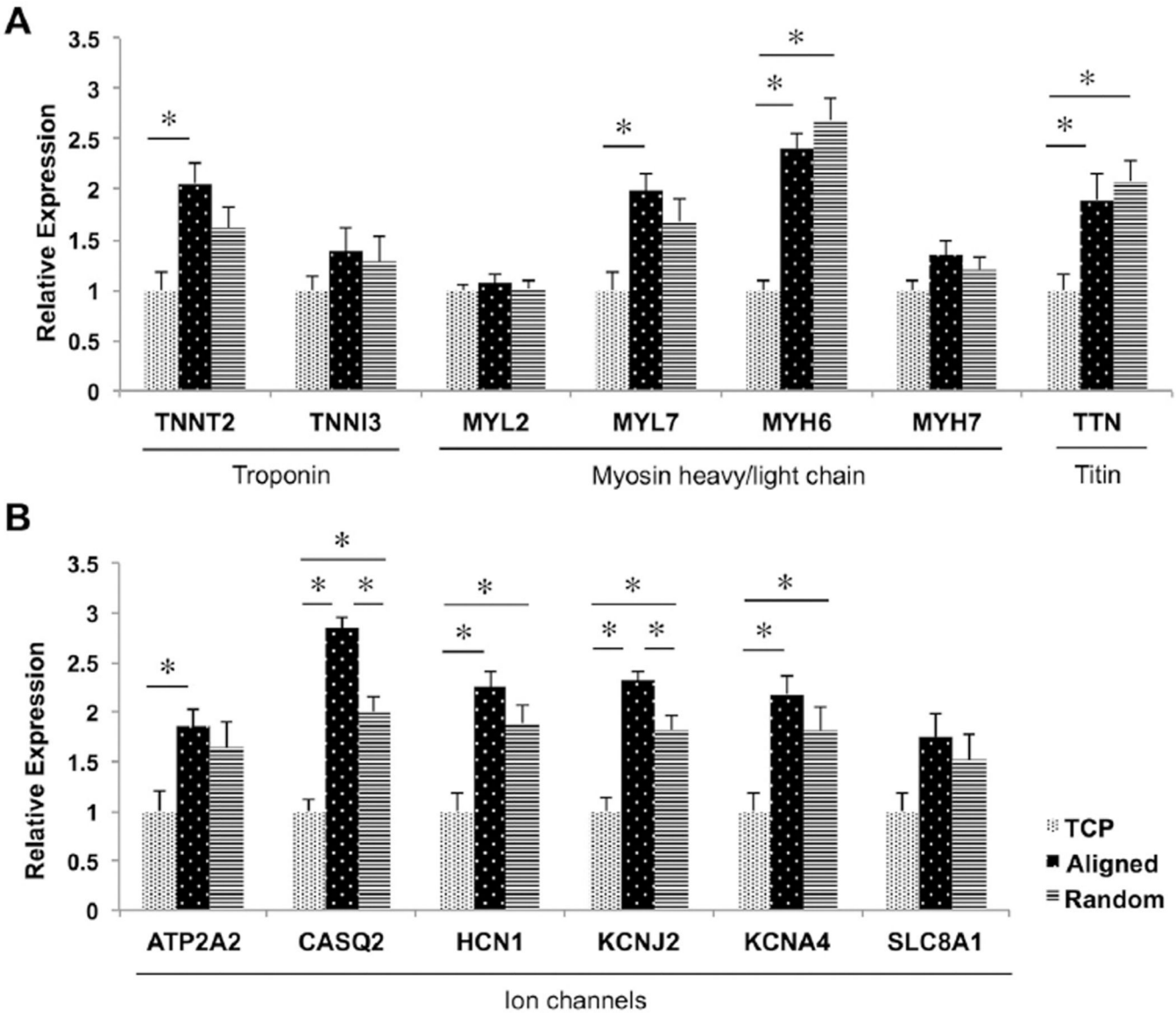

Fig. 5.

Relative expression of genes encoding (A) structural proteins and (B) ion channels or calcium handing proteins in hPSC-CMs cultured on the three substrates for 2 weeks. n = 9 from three independent experiments. *: $p < 0.05$ by one-way ANOVA *post hoc* Tukey test.

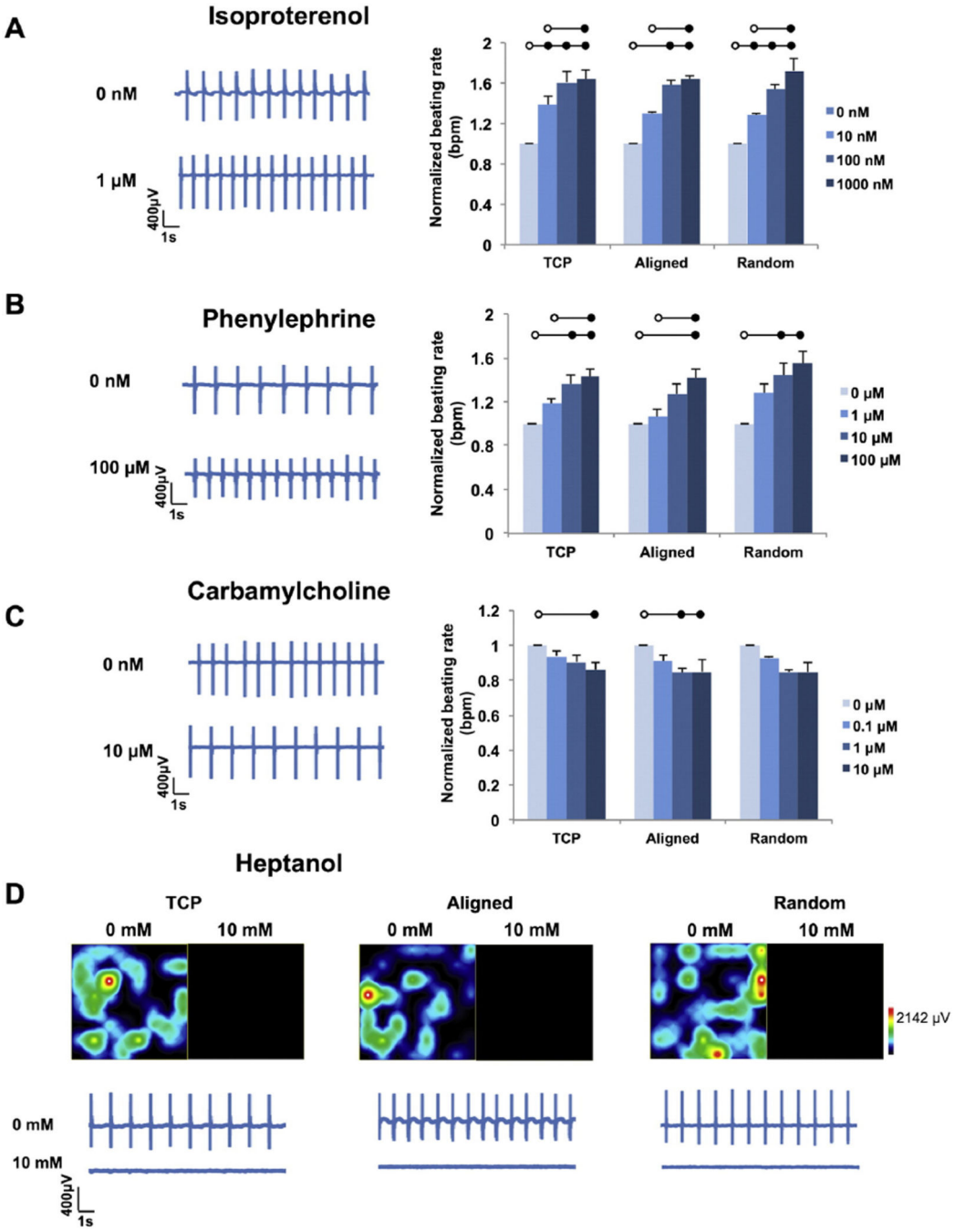

Fig. 6.

Pharmacological responses of hPSC-CMs to cardio-active compounds, (A) isoproterenol, (B) phenylephrine, (C) carbamylcholine, and (D) heptanol. For hPSC-CMs from cultures on all substrates, isoproterenol and phenylephrine increased the beating rates whereas carbamylcholine decreased the beating rates, and heptanol stopped the CM electrical activity. (A–C) Left, representative image of hPSC-CMs in a multielectrode array (MEA) chamber. Scale bar: 200 μm. Middle, representative MEA recordings in the beating rates of hPSC-CMs before and after incubation with various compounds. Right, normalized beating

rates of hPSC-CMs in response to various drugs at a dose-dependent manner. Data represented hPSC-CMs on 2–6 MEA chambers in three independent experiments. Black dot: $p < 0.05$ versus white dot by two-way ANOVA *post hoc* Tukey test. (D) Representative images of the field potentials in hPSC-CMs plated in the MEA chambers (top) and the beating rates in hPSC-CMs (bottom) before and after incubation with 10 mM heptanol.

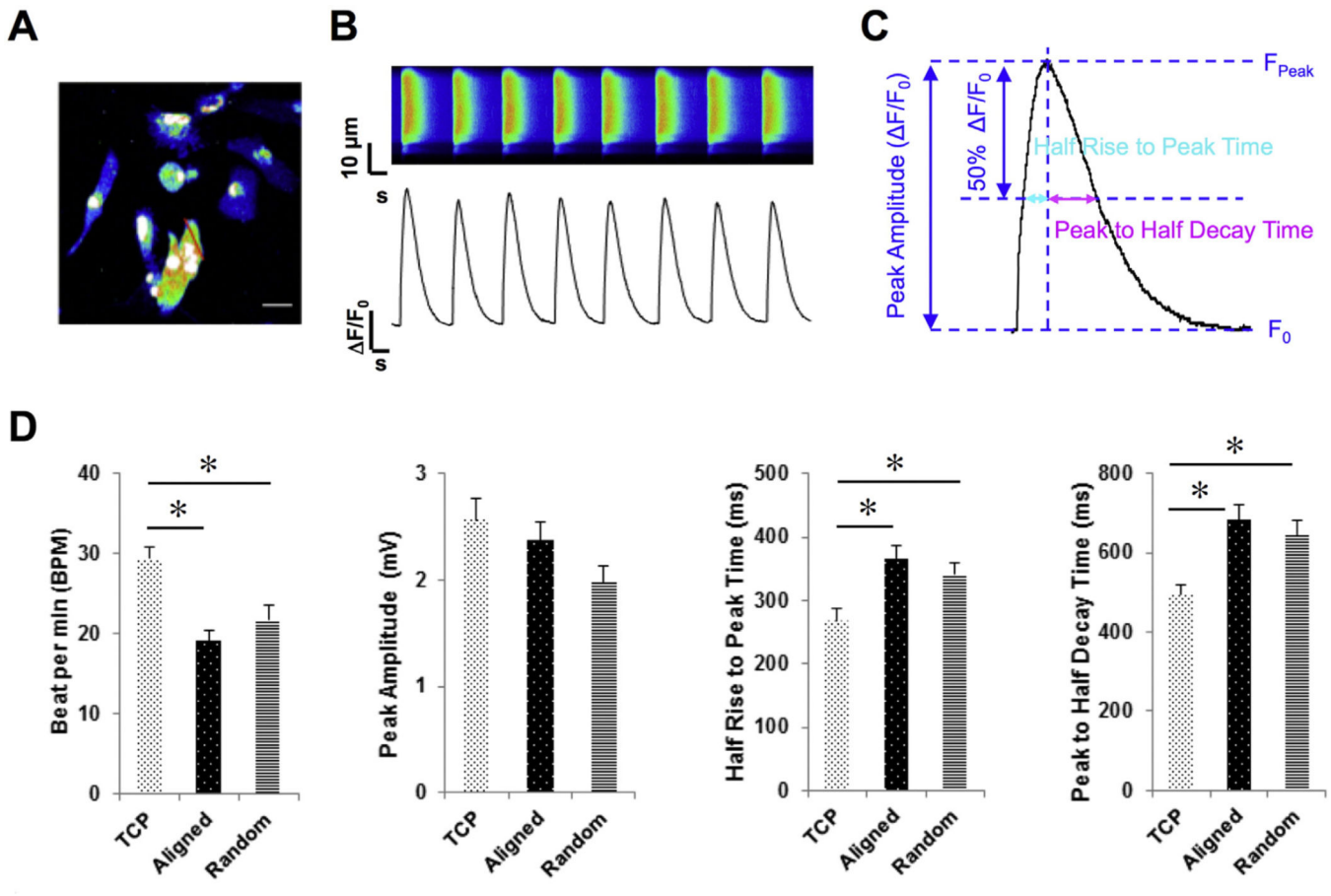

Fig. 7.

Calcium transient analysis of hPSC-CMs from cultures on the three substrates. (A) Representative line-scan of time-lapse calcium imaging in hPSC-CMs loaded with the intracellular calcium indicator Fluo-4 AM where increased calcium activity was indicated by the color change from blue to green, to red. The red line indicated the location where line-scan was performed. Scale bar: 20 µm. (B) Representative recording of spontaneous calcium transient. (C) Schematic illustration of the measurements of calcium transient parameters. (D) Summary of calcium transient frequency (beats per min), peak amplitude, half rise to decay time, and peak to half decay time among hPSC-CMs cultured on TCPs (n = 52), aligned (n = 62) and random fibrous scaffolds (n = 58) from three independent experiments. *: $p < 0.05$ via Kruskal–Wallis one-way ANOVA on ranks using Dunn's method for pairwise multiple comparisons.